Journal of Hydro-environment Research 31 (2020) 41–47

Contents lists available at ScienceDirect

Journal of Hydro-environment Research

journal homepage: www.elsevier.com/locate/jher

Positive surge propagating in an asymmetrical canal

Urvisha Kiri, Xinqian Leng[1], Hubert Chanson[*,2]

The University of Queensland, School of Civil Engineering, Brisbane, QLD 4072, Australia

ARTICLE INFO

Keywords:
Positive surge
Compression waves
Open channels
Asymmetrical canal
Physical modelling
Transient three-dimensional free-surface features

ABSTRACT

A positive surge is an unsteady open channel flow motion characterised by a sudden rise in water surface elevation. The literature is focused primarily on rectangular channels. Herein, the free-surface features of positive surges propagating upstream were investigated in an asymmetrical canal. The surge propagation was a three-dimensional unsteady flow motion, resulting in a complicated transient secondary motion compared to positive surge propagating in rectangular canals. The present results may be relevant to surge propagation in man-made trapezoidal canals and natural irregular-shaped channels.

1. Presentation

A positive surge is an unsteady, rapidly-varied and highly turbulent open channel flow, characterised by a sudden rise in water surface elevation (Henderson, 1966; Liggett, 1994; Chanson, 2004). Environmental applications encompass tidal bores and tsunami propagation upriver (Tricker, 1965; Lighthill, 1978; Tanaka et al., 2012). Industrial situations include rejection surges in hydropower and water supply canals (Favre, 1935; Cunge, 1966). Recent experimental works demonstrated the intense mixing induced by the surge propagation, and coupling between free-surface deformation and turbulent Reynolds stress tensor (Khezri and Chanson, 2012; Leng and Chanson, 2016).

To date, most research focused primarily on positive surges propagating in rectangular channels, except for limited free-surface observations in symmetrical trapezoidal channels (Sandover and Taylor, 1962; Benet and Cunge, 1971; Treske, 1994) and numerical computations in non-rectangular channels (Mitchell, 2010; Shi et al., 2014). The literature on positive surges and jumps in asymmetrical channels is very limited, despite the relevance to natural channels. Additionally a number of physical studies were conducted in stationary hydraulic jumps in non-rectangular symmetrical canals (Mohed and Sharp, 1971; Wanoschek and Hager, 1989).

Herein, the upstream translation and free-surface characteristics of positive surges are investigated in an asymmetrical prismatic channel. The geometry was selected as a simplified distorted scaling of a natural channel where tidal bores are observed. It is shown that the surge propagation is a three-dimensional unsteady flow motion, with complicated free-surface features, compared to positive surge propagation in rectangular canals. Its properties are developed, and physical observations are discussed.

2. Theoretical background

Called a hydraulic jump in translation, a positive surge is characterised by an abrupt front (Fig. 1). The surge front may be analysed using the equations of conservation of mass and momentum (Lighthill, 1978; Liggett, 1994). For a smooth horizontal irregular channel, the system of equations provides a relationship between the surge Froude number and the ratio of conjugate depth (Chanson, 2012). In a system of reference in translation with the surge, it gives:

$$\frac{A_2}{A_1} = \frac{1}{2} \times \frac{\sqrt{\left(2 - \frac{B'}{B}\right)^2 + 8\frac{\frac{B'}{B}}{\frac{B_1}{B}} Fr_1^2} - \left(2 - \frac{B'}{B}\right)}{\frac{B'}{B}} \quad (1)$$

where A is the channel cross-sectional area measured perpendicular to the flow direction, B_1 is the initial free-surface width, the subscripts 1 and 2 refer to the flow conditions immediately before and after the surge respectively (Fig. 1B), Fr_1 is the surge Froude number:

$$Fr_1 = \frac{U + V_1}{\sqrt{g\frac{A_1}{B_1}}} \quad (2)$$

with V the flow velocity positive downstream, U the surge celerity positive upstream, g the gravity acceleration. In Eq. (1), B and B' are

* Corresponding author.
E-mail address: h.chanson@uq.edu.au (H. Chanson).
[1] ORCID: X. Leng 0000-0001-8472-7925
[2] ORCID: H. Chanson 0000-0002-2016-9650

https://doi.org/10.1016/j.jher.2020.04.002
Received 20 May 2018; Received in revised form 11 October 2018; Accepted 27 April 2020
Available online 07 May 2020
1570-6443/

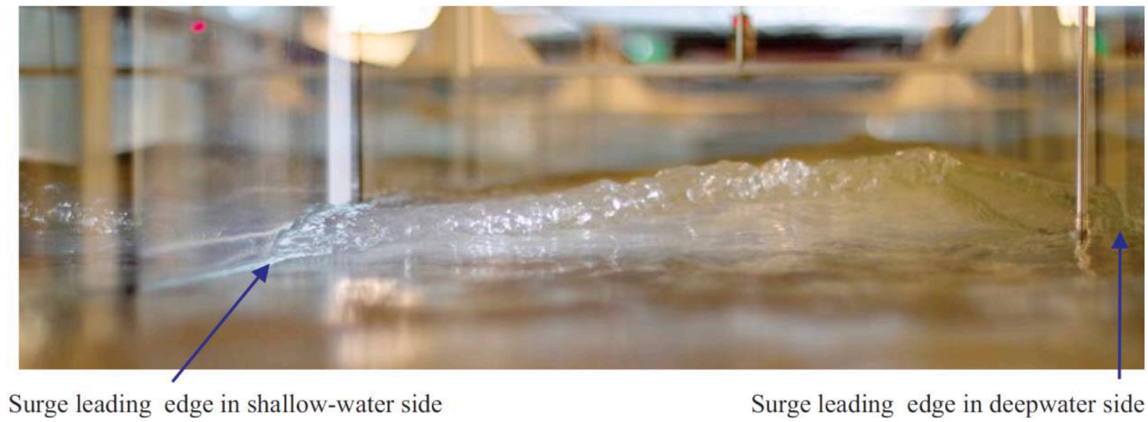

(A) Three-dimensional surge propagating upstream, looking downstream - Flow conditions: Q = 0.055 m^3/s, Fr_1 = 1.3, d_1/D = 1.17 m, λ = 5

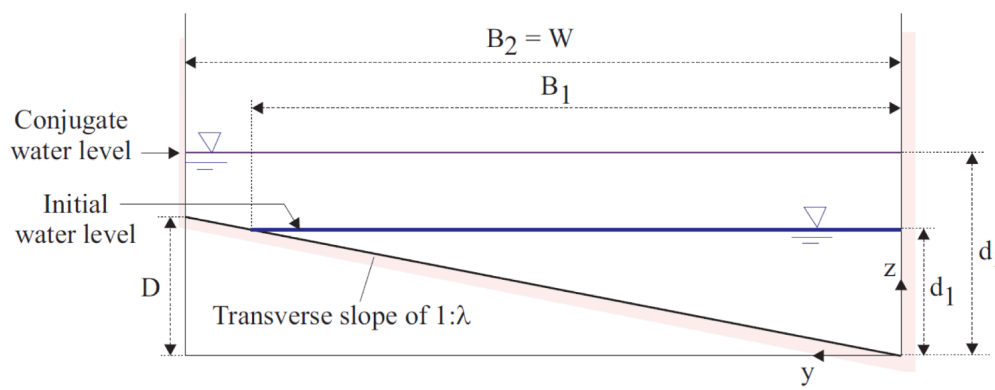

(B) Definition sketch looking downstream - In the present study: λ = W/D = 5

Fig. 1. Positive surge propagation in an asymmetrical channel.

characteristic widths related to the cross-sectional shape:

$$B = \frac{A_2 - A_1}{d_2 - d_1} \tag{3}$$

$$B' = \frac{\int_{A_1}^{A_2} \int g(d_2 - y)dA}{\frac{1}{2}g(d_2 - d_1)^2} \tag{4}$$

with d the flow depth (Fig. 1B). Eq. (1) gives an analytical expression of the ratio of cross-sectional areas A_2/A_1 as a function of the surge Froude number and dimensionless cross-sectional characteristics B'/B and B_1/B.

In the present study, the propagation of positive surges was investigated in an asymmetrical non-rectangular channel with a transverse bed slope (Fig. 1B). The initial flow cross-section area and free-surface width are respectively:

$$A = \frac{1}{2} \times \lambda \times d^2 \quad \& \quad B = \lambda \times d \qquad d_1 < D \tag{5a}$$

$$A = W \times \left(d - \frac{D}{2}\right) \quad \& \quad B = W \qquad d_1 > D \tag{5b}$$

where λ^{-1} is transverse slope of the bed, W is the total width and D is the transverse difference in bed elevation, i.e. D = W/ λ (Fig. 1B). For this geometry, three boundary conditions may occur depending upon the initial and new (conjugate) flow depths: (a) $d_1 < d_2 < D$, (b) $d_1 < D < d_2$, and (c) $D < d_1 < d_2$. Analytical solutions are detailed in Appendix I for all three cases. The third case is trivial, since B_1 = B = B' = B_2.

3. Physical study

New experiments were conducted in a 19 m long 0.7 m wide tilting flume, previously used by Leng and Chanson (2015, 2016) with a rectangular cross-section. The channel bed was modified with the installation of a 1 V:5H transverse slope (i.e. λ = 5), made out of PVC (Fig. 1B & 2) and the longitudinal bed slope was quasi-horizontal (S_o = 0.22%). The channel geometry was based upon a simplified, distorted scaling of the Arcins Channel of the Garonne River, France, where extensive field observations were conducted (Chanson et al., 2011; Keevil et al., 2015; Reungoat et al., 2014, 2017a, 2017b). The natural channel was about 70 m wide with a 1:35 (λ ~ 35) transverse slope. In laboratory, the horizontal scaling ratio was X_r ~ 100:1 and the vertical scaling ratio was Z_r ~ 15:1.

The laboratory water was supplied by a feeding tank, in which the flow

Table 1
Experimental investigation of positive surge propagation in an asymmetrical canal.

Q	d_1	S_o	h	U	Fr_1
(m^3/s)	(m/s)		(m)	(m/s)	
0.100	0.207	0.002216	0–0.067	0.2–1.1	1.3–1.8
0.055	0.167			0.67	1.53
0.030	0.130			0.4–0.6	1.11–1.15

Notes: d_1: initial water depth; Fr_1: surge Froude number; h: Tainter gate opening after closure; S_o: bed slope; U: surge celerity.

was streamlined before entering a smooth 3D convergent leading to the 0.7 m wide flume. A fast closing gate was located at the downstream end of the channel: x = 18.1 m, where x is measured from the test section's upstream end. The experimental flow conditions are summarised in Table 1 where Q is the initial water discharge, S_o is the bed slope, h is the Tainter gate opening after closure, U is the transverse-averaged surge celerity positive upstream. High-speed video observations were performed using a digital camera Casio™ Exlim EX-10 set at 120 fps. Photographs were taken during the surge propagation, using a dSLR Pentax™ K-3 with prime lenses, producing photographs with a low degree of distortion.

In steady flows, the water depths were measured using rail mounted pointer gauge. The unsteady surge free-surface pattern was recorded using a series of eight acoustic displacement meters (ADMs) Microsonic™ Mic + located along and above the channel, with two ADMs along the centreline at x = 6.96 m and x = 9.96 m, and six ADMs at x = 8.5 m, spaced evenly in the transverse direction: y = 0.100 m, 0.200 m, 0.300 m, 0.400 m, 0.500 m and 0.600 m (Fig. 2). The six ADM units located at x = 8.5 m were set up such that they emitted signals in a multiplex fashion to prevent signal interference between adjacent sensors. Additionally, two ADMs were placed immediately upstream and downstream of the Tainter gate to capture the gate closure time. All ADM sensors were calibrated against rail mounted pointer gauge water depth data. For each unsteady experiment, the free-surface elevation measurements were sampled at 100 Hz. The surge celerity was measured with the acoustic displacement meters located at x = 6.96 m, 8.5 m and 9.96 m, and the data were checked against video-camera recordings through the glass-sidewalls.

Experiments were performed with initially-steady discharges Q = 0.030 m^3/s to 0.10 m^3/s (Table 1). The positive surges were generated by the fast closure of the Tainter gate and the surge propagated upstream against the initially-steady flow (Fig. 1A). Although the generation process was highly turbulent, the surge formed very rapidly immediately after gate closure and became fully-developed, i.e. a translating surge, for x < 15 m. Its shape and mean properties did not vary along the sampling section (6.96 m < x < 9.96 m). For each flow condition, experiments were repeated 25 times and the results were ensemble-averaged.

4. Results (1) flow patterns

Visual observations were conducted with initial depths d_1 ranging from < 0.13 m to > 0.2 m, d_1 being measured next to the right sidewall (Fig. 1B). Basic dimensional considerations suggested that the surge flow patterns are functions of the surge Froude number $(V_1 + U)/(g \times A_1/B_1)^{1/2}$, the initial relative depth d_1/D and the surge Reynolds number $\rho \times (V_1 + U) \times A_1/B_1/\mu$, where D is the maximum height of the transverse bed slope: D = 0.140 m (Fig. 1B). Within the range of investigated flow conditions (Table 1), the present observations showed that the flow features were mostly affected by the Froude number and initial relative depth. Fig. 1A presents a photograph of the advancing surge. Appendix II lists a series of movies available in the Digital Appendix. Appendix III refers to the supplementary material with comparative photographs of positive surge propagation in rectangular and asymmetrical canal configurations for some identical flow condition.

For $Fr_1 > 1.5$ and $d_1/D > 1.5$, the positive surge was breaking (Digital Appendix, movie Video_9.mov). The roller region was quasi-two-dimensional. Air bubble entrainment was observed through the glass sidewalls, with the bubble being entrapped by and convected in the large-scale coherent structures of the roller shear layer.

For all other flow conditions, i.e. $Fr_1 < 1.5$ or $d_1/D < 1.5$, the surge was undular with some breaking, and marked three-dimensional features. Namely, the positive surge was undular in the deep-water (right) side, and some breaking was observed towards the left sidewall in the shallow-water section. The surge leading edge arrived first in the shallow-water side and trailed in the deep-water section (Digital Appendix Movie CIMG2384.MOV). That is, the surge front propagated upstream at an angle to the sidewall, although the surge celerity was the same on both sides of the flume. Complicated flow features were observed behind the surge front, with surface scars implying transverse mixing in the wake of the shallow-water surge front. For $Fr_1 < 1.5$ and $Re_1 < 1.5 \times 10^5$, the surge features were three-dimensional. In the shallow-water section, the breaking bore front was characterised by a sharp increase in the free-surface elevation and the roller region was associated with air bubble entrainment. In the deep-water side, the undular surge front was characterised by a gradual increase in the free-surface elevation, sometimes with partial breaking. Quasi-periodic secondary currents were observed behind the surge front. Across the channel width, from the deeper section to the shallower section, the undulation amplitude a_w, wave length L_w and wave period decreased, before transitioning to a breaking surge. Detailed

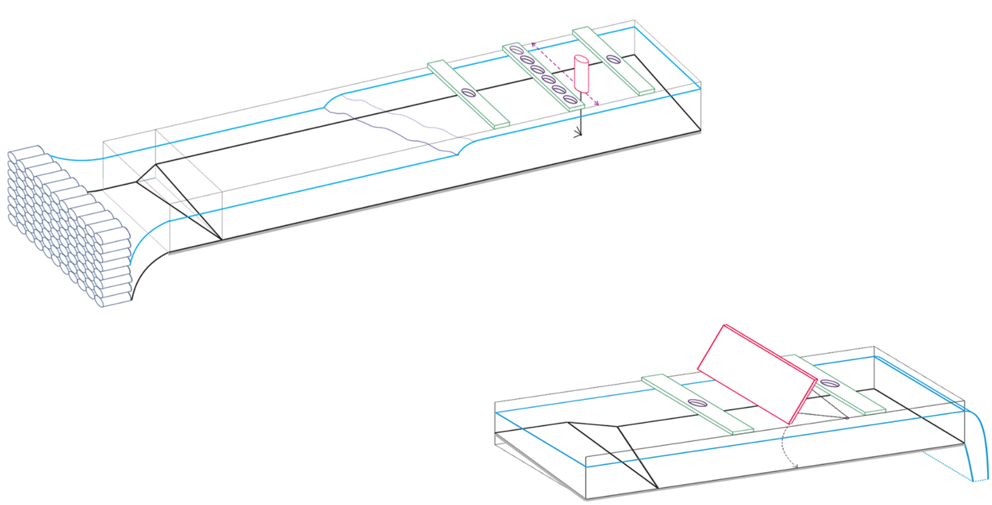

Fig. 2. Three-dimensional sketch of the experimental channel and experimental setup, with initially steady flow direction from left to right. Top: intake structure and upstream end of flume; Bottom: downstream end of flume and Tainter gate.

Table 2
Positive surge characteristics across the channel for several discharges and gate openings.

Q (m^3/s)	H (m)	Fr_1	y = 0.100 m			y = 0.200 m			y = 0.300 m			y = 0.400 m			y = 0.500 m			y = 0.600 m		
			Period (s)	a_w (mm)	L_w (m)	Period (s)	a_w (mm)	L_w (m)	Period (s)	a_w (mm)	L_w (m)	Period (s)	a_w (mm)	L_w (m)	Period (s)	a_w (mm)	L_w (m)	Period (s)	a_w (mm)	L_w (m)
0.031	0	1.61	1.88	26.51	1.06	1.66	10.34	0.93	1.46	8.65	0.82	Breaking			Breaking			Breaking		
0.0503	0	1.64	1.61	17.93	1.06	1.59	19.13	1.05	1.56	13.38	1.03	1.40	8.44	0.92	Breaking			Breaking		
0.0543	0	1.58	1.28	22.59	0.82	1.21	23.78	0.78	1.18	21.30	0.76	1.27	10.59	0.82	Breaking			Breaking		
0.0546	0.032	1.31	1.39	15.36	0.62	1.46	26.87	0.65	1.56	21.20	0.69	1.55	15.62	0.69	1.51	6.41	0.67	Breaking		
0.1017	0	1.66	Breaking			Breaking			Breaking			Breaking			Breaking			Breaking		
0.1017	0.055	1.30	1.33	11.39	0.59	1.25	11.36	0.56	1.21	10.62	0.54	1.21	8.55	0.54	Breaking			Breaking		

Notes: a_w: free-surface undulation amplitude; h: Tainter gate opening after closure; L_w: free-surface undulation wave length; Period: free-surface undulation period; y: transverse distance from the right sidewall.

experimental observations are presented in Table 2, including the surge characteristics at several transverse locations for several flow conditions. Despite the three-dimensional features, the conjugate free-surface elevation was the same across the channel width.

For $d_1/D < 1$, visual observations highlighted characteristic three-dimensional features, with strong transverse mixing illustrated by large-scale vortices and surface scars behind the surge front (Digital Appendix, movie CIMG2384.mov). Dye was injected in the initially steady flow and its dispersion in the positive surge was visualised. The dye injection experiments showed drastically different conjugate motions between the left and right sides. In the deeper side (right), the conjugate flow motion continued to flow downstream, while, in the shallower (left) side, the flow changed direction after the surge, moving upstream (Digital Appendix movie CIMG3467.mov). The transient flow pattern is sketched in Fig. 3. The unsteady flow pattern led to some complicated secondary currents and shear zone about the channel centreline. The occurrence of flow reversal in the shallower part of the asymmetrical canal was a major difference in comparison to similar experiments in rectangular channels.

Altogether, the present findings presented some similarity with positive surge propagation in a compound channel (Pan and Chanson, 2015). The current observations showed also some similarity with field observations of tidal bore in natural trapezoidal channels, e.g. Garonne River at Arcins (Keevil et al., 2015; Reungoat et al., 2017a).

5. Results (2) Free-surface observations

Free-surface measurements were conducted at × = 8.5 m for a range of flow conditions at various transverse locations, and the results were ensemble-averaged. Fig. 4 presents three-dimensional ensemble-averaged free-surface measurements of the propagating surge, in terms of the ensemble-median water depth. In Fig. 4, the longitudinal axis is the dimensionless time $t(gA_1/B_1)^{1/2}$. The free-surface fluctuations were characterised in terms of the difference between the third and first quartiles $d_{75\text{-}25}$. For a Gaussian distribution of ensemble-averaged data, this inter-quartile range $d_{75\text{-}25}$ would be equal to 1.3 times the standard deviation (Spiegel, 1972). Leng and Chanson (2015) showed that the

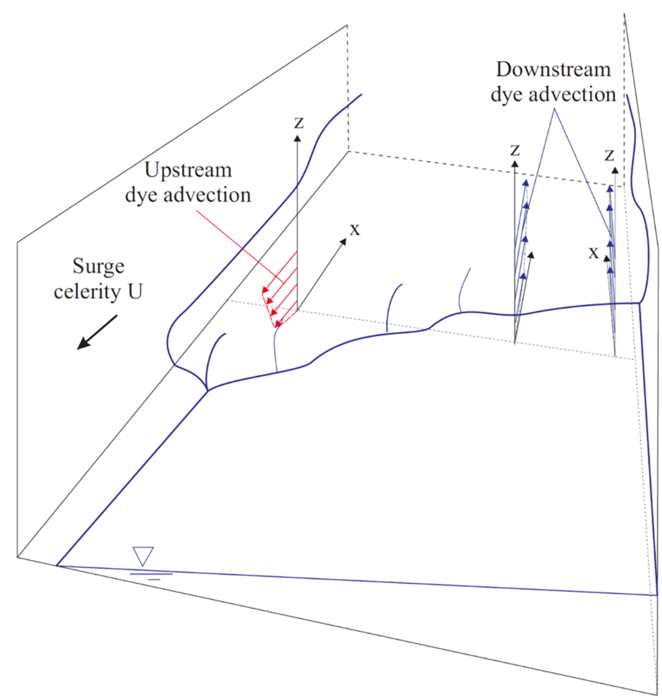

Fig. 3. Sketch of transient velocity field behind a positive surge in the asymmetrical channel for Q = 0.030 m^3/s.

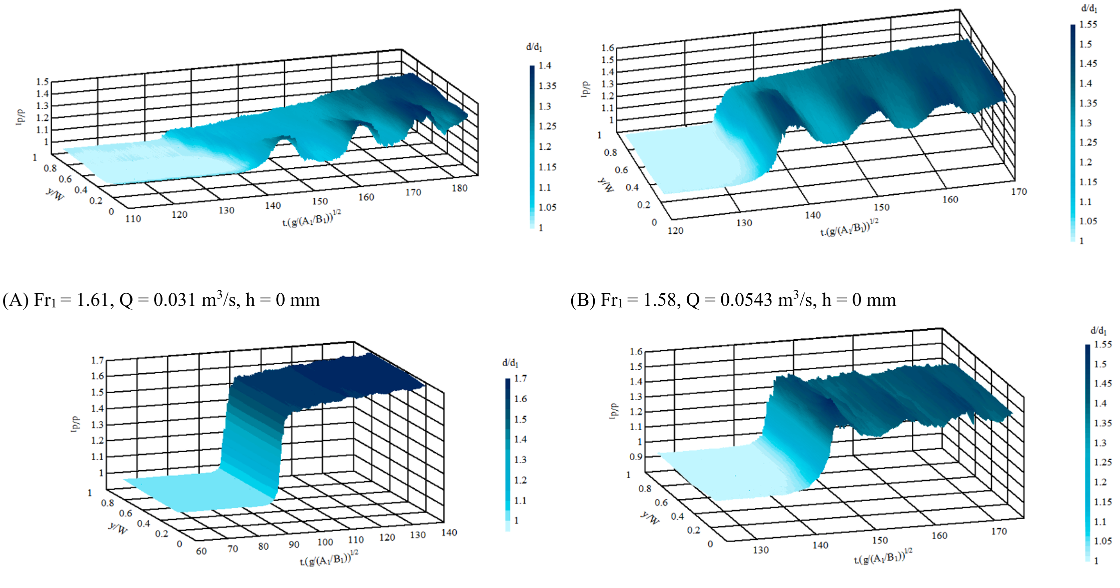

(A) $Fr_1 = 1.61$, $Q = 0.031$ m^3/s, h = 0 mm

(B) $Fr_1 = 1.58$, $Q = 0.0543$ m^3/s, h = 0 mm

(C) $Fr_1 = 1.66$, $Q = 0.1017$ m^3/s, h = 0 mm

(D) $Fr_1 = 1.30$, $Q = 0.1017$ m^3/s, h = 0.055 m

Fig. 4. Dimensionless time-variations of three dimensional ensemble-averaged free-surface measurements during surge propagation. Measurements at $x = 8.5$ *m*.

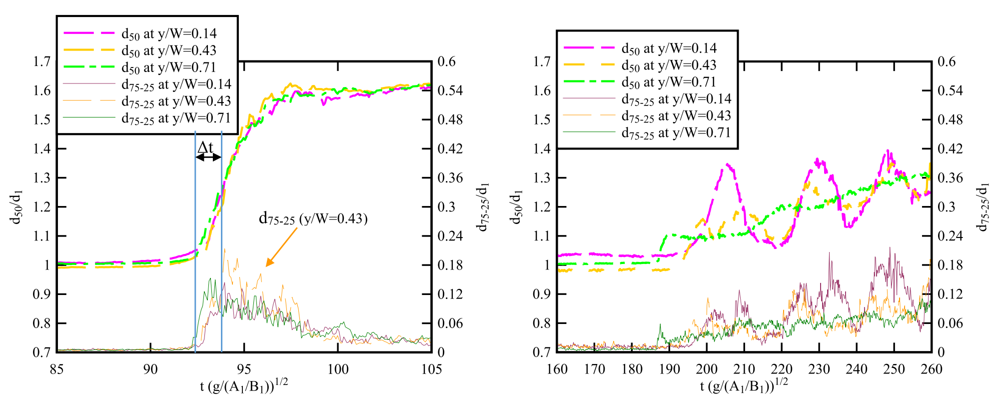

(A) $Fr_1 = 1.67$, $Q = 0.1017$ m^3/s, h = 0 m, $d_1 = 0.209$ m

(B) $Fr_1 = 1.66$, $Q = 0.0308$ m^3/s, h = 0 m, $d_1 = 0.127$ m

Fig. 5. Dimensionless time variation of median free-surface elevation and free-surface fluctuations across the channel.

inter-quartile range data compared favourably with free-surface fluctuations observed in breaking bores and stationary hydraulic jumps. Fig. 5 presents typical dimensionless ensemble-median water elevation d_{50}/d_1 and dimensionless fluctuation in water elevation $d_{75\text{-}25}/d_1$ during the surge passage for discharges $Q = 0.1017$ m^3/s and 0.055 m^3/s.

All free-surface elevation data showed a rapid rise in water elevation at all transverse locations (Figs. 3 & 4). Similarly, the free-surface fluctuation data showed a marked increase, by an order of magnitude, immediately following the arrival of the surge, characterising the highly turbulent process. With a breaking bore, the surge front passage showed a sharp increase in the free-surface fluctuations immediately following the arrival of the surge, as shown in Fig. 5A. Free-surface fluctuations in undular surge sections showed an increase, followed by some quasi-periodic oscillation with the same period as the secondary free-surface elevation oscillations, but out of phase, as shown in Fig. 5B. The maxima and minima in free-surface fluctuations roughly corresponded to the greatest rate of change in the free-surface elevation. Fig. 5B illustrates the fluctuations in free-surface elevation during the passage of an undular surge with slight breaking.

For all experiments, the maximum free-surface fluctuations were observed with a time lag Δt, following the passage of the surge's leading edge, as illustrated on Fig. 5A for the location $y/W = 0.43$. This phenomenon has been previously observed by Leng and Chanson (2016). The time lag between the maximum fluctuation and surge's leading edge, and the magnitude of the maximum fluctuation differed across the channel, suggesting strongly three-dimensional free-surface features.

6. Discussion

The free-surface data were compared to past laboratory studies in rectangular and trapezoidal channels, past field investigations in man-made canals and natural channels, and analytical solutions. Key features of the positive surge included the conjugate cross-section area A_2 and characteristics widths (B_2, B_1, B and B') (section 2). The full data set of positive surge features is reported in Kiri et al. (2018). Theoretical considerations showed that the dimensionless conjugate area, A_2/A_1 is a function of the surge Froude number (Eq. (1)). Fig. 6 presents a comparison between present experimental data and theoretical results. Fig. 6 also includes field investigations of tidal bores in irregular channels, a field investigation in hydropower canal, and laboratory studies in rectangular and trapezoidal channels. (In rectangular channels, the ratio of the conjugate depth d_2/d_1 is equal to the ratio of the conjugate area A_2/A_1.) Details are summarised in the figure caption. In addition, the Bélanger equation for rectangular channel is shown as a solid line.

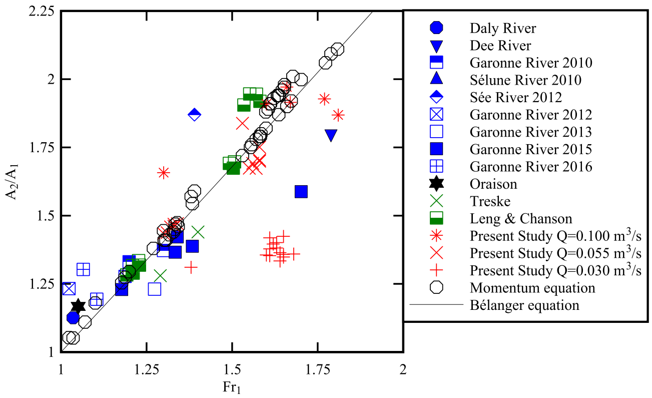

Fig. 6. Ratio of conjugate cross-section areas A_2/A_1 as a function of the surge Froude number Fr_1 for positive surges propagating in irregular canals. Comparison between field investigations, laboratory experiments, momentum equation for irregular channels (Eq. (1)), and traditional Bélanger equation for rectangular canals.

Data set name	Reference	Description	Channel cross-section
Daly River	Wolanski et al. (2004)	Tidal bore (Field)	Trapezoidal, irregular
Dee River	Simpson et al. (2004)	Tidal bore (Field)	Trapezoidal, irregular
Garonne River 2010	Chanson et al. (2011)	Tidal bore (Field)	Trapezoidal, asymmetrical
Sélune River 2010	Mouaze et al. (2010)	Tidal bore (Field)	Triangular, asymmetrical
Sée River 2012	Furgerot et al. (2013)	Tidal bore (Field)	Trapezoidal, irregular
Garonne River 2012	Reungoat et al. (2014)	Tidal bore (Field)	Trapezoidal, asymmetrical
Garonne River 2013	Keevil et al. (2015)	Tidal bore (Field)	Trapezoidal, asymmetrical
Garonne River 2015	Reungoat et al. (2017a)	Tidal bore (Field)	Trapezoidal, asymmetrical
Garonne River 2016	Reungoat et al. (2017b)	Tidal bore (Field)	Trapezoidal, asymmetrical
Oraison	Ponsy and Carbonnell (1966)	Hydropower canal (Field)	Trapezoidal, symmetrical
Treske	Treske (1994)	Laboratory	Trapezoidal, symmetrical
Leng & Chanson	Leng and Chanson (2016)	Laboratory	Rectangular
Present study	Present study	Laboratory	Trapezoidal/triangular, asymmetrical

Overall the present data compared favourably to the analytical solution of the momentum equation (Eq. (1)), despite some scatter. An increase in the surge Froude number was associated with an increase in the ratio of conjugate areas. The experimental data for the higher discharges followed closely results from previous studies. For the lowest discharge when the initial cross section was triangular, however, the present data deviated from field observations and analytical solution. The trend is not currently explained, although the data were checked carefully.

7. Conclusion

When a positive surge propagates in an asymmetrical canal, a key feature is the three-dimensional unsteady flow motion. This aspect was documented herein based upon detailed free-surface observations performed in a 19 m long 0.7 m wide canal, equipped with a 1 V:5H transverse bed slope, corresponding to a simplistic distorted scale model of the Arcins Channel (France) where tidal bores are seen. Unsteady measurements were conducted using acoustic displacement meters and the results were ensemble averaged.

The positive surge flow pattern was a function of the surge Froude number Fr_1 and relative initial flow depth d_1/D. During the propagation of the surge front, the leading edge of the surge arrived first in the shallow-water section. This resulted in three-dimensional turbulent mixing associated with the formation of surface scars and complicated transient secondary motion behind the surge front. While the present observations presented some similarity to earlier observations in rectangular channels, a major difference was the three-dimensional nature of the surge front in the asymmetrical non-rectangular channel.

The present findings may be directly relevant to positive surge propagation in man-made trapezoidal waterways and natural irregular-shaped channels.

Acknowledgments

The authors thank Professor Rollin Hotchkiss (Brigham Young University, USA) and Dr Oscar Castro-Orguaz (University of Cordoba, Spain) for valuable comments. They acknowledge helpful inputs of Professor Pierre Lubin (University of Bordeaux, France). The authors acknowledge the financial supports of the Australian Research Council (Grant DP120100481), and the technical assistance of Jason Van Der Gevel and Matthews Stewart (The University of Queensland). Finally the authors are grateful to the reviewers for their constructive comments.

Appendix I. Analytical solutions for an asymmetrical channel (shown in Fig. 1)

	$d_1 < d_2 < D$	$d_1 < D < d_2$	$D < d_1 < d_2$
B =	$\frac{1}{2} \times \lambda \times (d_1 + d_2)$	$\frac{B_2 \times \left(d_2 - \frac{D}{2}\right) - \frac{1}{2} \times \lambda \times d_1^2}{d_2 - d_1}$	$B_1 = B_2 = W$
B' =	$\frac{\lambda \times \rho \times g \times \left(\frac{d_2^3}{6} - \frac{d_1^2}{6} \times (3 \times d_2 - 2 \times d_1)\right)}{\frac{1}{2} \times \rho \times g \times (d_2 - d_1)^2}$	$\frac{\frac{1}{2} \times (d_2 - D)^2 \times B_2 + \lambda \times \left(\frac{D^2}{6} \times (3 \times d_2 - 2 \times D) - \frac{d_1^2}{6} \times (3 \times d_2 - 2 \times d_1)\right)}{\frac{1}{2} \times (d_2 - d_1)^2}$	$B_1 = B_2 = W$

Appendix II. Movies of positive surge experiments in an asymmetrical canal (Digital Appendix)

Video observations of the positive surge experiments were carried out using a digital camera Pentax™ K-3 (50 fps, resolution: 1980p × 1080p) and a digital camera Casio™ Exilim Ex10 (30 fps, resolution: 1980p × 1080p; 120 fps, resolution: 640p × 480p). Table A1 describes each video movie available in the digital appendix.

Appendix III. Supplementary material: comparative photographs of positive surge propagation in rectangular and asymmetrical canals

Table A1
Video observations of positive surge propagation in an asymmetrical canal.

Filename	Camera	Description
IMGP4248.mov	Pentax™ K-3 with lens Carl Zeiss 28 mm f2 Frame rate: 50 fps	Positive surge generation induced by the rapid Tainter gate closure. Gate closure sequence (h = 0). Flow conditions: Q = 0.032 m^3/s, S_o = 0, h = 0 m. Movie duration: 5 s.
Video_9.mov	Casio™ Exilim Ex10 Frame rate: 120 fps	Breaking surge propagation at x = 8.6 m. Flow conditions: Q = 0.10 m^3/s, Fr_1 = 1.5–1.7. Movie duration: 21 s (replay). Movie replayed at 30 fps - the 120 fps movie is replayed at 25% normal speed.
CIMG2384.MOV	Casio™ Exilim Ex10 Frame rate: 30 fps	Three-dimensional surge propagation at x = 8.6 m, viewed through the right sidewall. Flow conditions: Q = 0.03 m^3/s. Movie duration: 3 s
CIMG3467.MOV	Casio™ Exilim Ex10 Frame rate: 30 fps	Three-dimensional surge propagation with dye injection. Flow conditions: Q = 0.032 m^3/s, S_o = 0.002216, Fr_1 = 1.6–1.7, d_1/D = 0.93. Movie duration: 23 s.

Appendix B. Supplementary data

Supplementary data to this article can be found online at https://doi.org/10.1016/j.jher.2020.04.002.

References

Benet, F., Cunge, J.A., 1971. Analysis of experiments on secondary undulations caused by surge waves in trapezoidal channels. J. Hydraul. Res., IAHR 9 (1), 11–33.

Chanson, H., 2004. The hydraulics of open channel flow: an introduction, second ed., Butterworth-Heinemann, Oxford, UK, 630 pages.

Chanson, H., 2012. momentum considerations in hydraulic jumps and bores. J. Irrigation Drainage Eng., ASCE 138 (4), 382–385.

Chanson, H., Reungoat, D., Simon, B., Lubin, P., 2011. High-frequency turbulence and suspended sediment concentration measurements in the Garonne River Tidal Bore. Estuar. Coast. Shelf Sci. 95 (2–3), 298–306. https://doi.org/10.1016/j.ecss.2011.09.012.

Cunge, J.A., 1966. Comparaison des résultats des essais d'intumescences effectués sur le modèle réduit et sur le modèle mathématique du canal Oraison-Manosque. La Houille Blanche (1), 55–70. https://doi.org/10.1051/lhb/1966003.

Favre, H., 1935. Etude Théorique et Expérimentale des Ondes de Translation dans les Canaux Découverts. ('Theoretical and Experimental Study of Travelling Surges in Open Channels.), Dunod, Paris, France (in French).

Furgerot, L., Mouaze, D., Tessier, B., Perez, L., Haquin, S., 2013. Suspended sediment concentration in relation to the passage of a Tidal Bore (Sée River Estuary, Mont Saint Michel, NW France). In: Proc. Coastal Dynamics 2013, Arcachon, France, 24–28 June, pp. 671–682.

Henderson, F.M., 1966. Open Channel Flow. MacMillan Company, New York, USA.

Keevil, C.E., Chanson, H., Reungoat, D., 2015. Fluid flow and sediment entrainment in the Garonne River Bore and Tidal Bore Collision. Earth Surf. Proc. Land. 40 (12), 1574–1586. https://doi.org/10.1002/esp.3735.

Khezri, Nazanin, Chanson, Hubert, 2012. Sediment inception under breaking tidal bores. Mech. Res. Commun. 41, 49–53. https://doi.org/10.1016/j.mechrescom.2012.02.010.

Kiri, U., Leng, X., Chanson, H., 2018. Positive surge propagation in a non-rectangular asymmetrical channel. Hydraulic Model Report No. CH110/18, School of Civil Engineering, The University of Queensland, Brisbane, Australia, 159 pages and 2 digital appendices incl. 5 movies.

Leng, X., Chanson, H., 2015. Breaking bore: physical observations of roller characteristics. Mech. Res. Commun. 65, 24–29. https://doi.org/10.1016/j.mechrescom.2015.02.008.

Leng, X., Chanson, H., 2016. Coupling between free-surface fluctuations, velocity fluctuations and turbulent reynolds stresses during the upstream propagation of positive surges, bores and compression waves. Environ. Fluid Mech. 16 (4), 695–719. https://doi.org/10.1007/s10652-015-9438-8. digital appendix.

Liggett, J.A., 1994. Fluid Mechanics. McGraw-Hill, New York, USA.

Lighthill, J., 1978. Waves in Fluids. Cambridge University Press, Cambridge, UK 504 pages.

Mitchell, S.B., 2010. Positive surge in trapezoidal and circular channels. Water Manag. 163 (WM4), 199–205.

Mohed, M.B., Sharp, J.J., 1971. Hydraulic jump in trapezoidal channels. Water Water Eng. 75, 8–11.

Mouaze, D., Chanson, H., Simon, B., 2010. Field measurements in the Tidal Bore of the Sélune River in the Bay of Mont Saint Michel (September 2010). Hydraulic Model Report No. CH81/10, School of Civil Engineering, The University of Queensland, Brisbane, Australia, 72 pages.

Pan, D.Z., Chanson, H., 2015. Physical modelling of Tidal Bore Dyke overtopping: implication on individuals' safety. In: Proc. 36th IAHR World Congress, The Hague, The Netherlands, 27 June–3 July, Theme 4, pp. 3824–3831.

Ponsy, J., Carbonnell, M., 1966. "Etude Photogrammétrique d'Intumescences dans le Canal de l'Usine d'Oraison (Basses-Alpes)." ('Photogrammetric Study of Positive Surges in the Oraison Powerplant Canal'.). Jl Soc Française de Photogram 22, 18–28 (in French).

Reungoat, D., Chanson, H., Caplain, B., 2014. Sediment processes and flow reversal in the Undular Tidal Bore of the Garonne River (France). Environ. Fluid Mech. 14 (3), 591–616. https://doi.org/10.1007/s10652-013-9319-y.

Reungoat, D., Leng, X., Chanson, H., 2017a. Successive impact of tidal bores on sedimentary processes: arcins channel, Garonne River. Estuar. Coast. Shelf Sci. 188, 163–173. https://doi.org/10.1016/j.ecss.2017.02.025.

Reungoat, D., Leng, X., Chanson, H., 2017b. Suspended sediment processes in the Garonne River Tidal Bore: arcins channel on 14-15 November 2016. Hydraulic Model Report No. CH108/17, School of Civil Engineering, The University of Queensland, Brisbane, Australia, 166 pages.

Sandover, J.A., Taylor, C., 1962. Cnoidal waves and bores. La Houille Blanche (3), 443–465. https://doi.org/10.1051/lhb/1962045.

Shi, J., Tong, C., Yan, Y., Luo, X., 2014. Influence of varying shape and depth on the generation of tidal bores. Environ. Earth Sci. 72, 2489–2496.

Simpson, J.H., Fisher, N.R., Wiles, P., 2004. Reynolds stress and TKE production in an Estuary with a Tidal Bore. Estuar. Coast. Shelf Sci. 60 (4), 619–627.

Spiegel, M.R., 1972. Theory and Problems of Statistics. McGraw-Hill Inc., New York, USA.

Tanaka, H., Nguyen, X.T., Umeda, M., Hirao, R., Pradjoko, E., Mano, A., Udo, K., 2012. Coastal and estuarine morphology changes induced by the 2011 Great East Japan Earthquake Tsunami. Coastal Eng. J. 54 (1). https://doi.org/10.1142/S0578563412500106. paper 1250010.

Treske, A., 1994. Undular bores (favre-waves) in open channels - experimental studies. J. Hydraul. Res. 32 (3), 355–370. https://doi.org/10.1080/00221689409498738.

Tricker, R.A.R., 1965. Bores, Breakers, Waves and Wakes. American Elsevier Publ. Co., New York, USA.

Wanoschek, R., Hager, W.H., 1989. Hydraulic jump in trapezoidal channel. J. Hydraul. Res., IAHR 27 (3), 429–446.

Wolanski, E., Williams, D., Spagnol, S., Chanson, H., 2004. Undular Tidal Bore dynamics in the Daly Estuary, Northern Australia. Estuar. Coast. Shelf Sci. 60 (4), 629–636.